INTERNATIONAL JOURNAL OF AUTOMOTIVE AND MECHANICAL ENGINEERING
ISSN: 2229-8649 e-ISSN: 2180-1606
VOL. 20, ISSUE 3, 2023, 10798 – 10807
DOI: https://doi.org/10.15282/ijame.20.3.2023.21.0835

RESEARCH ARTICLE

Impact of Deep Seawater on the Electrochemical Corrosion Performance of Hypoeutectic, Eutectic and Hypereutectic Al-Si Automotive Alloys

A. Abdullah Khan[1], A. Kabir Hossain[1] and M. S. Kaiser[2,*]

[1]Department of Mechanical Engineering, Bangladesh University of Engineering and Technology, Dhaka-1000, Bangladesh
[2]Innovation Centre, International University of Business Agriculture and Technology, Dhaka-1230, Bangladesh

ABSTRACT - Corrosion of aluminum alloys is a significant concern for shipbuilders to ensure the longevity of ocean vessels and equipment. Hence, the study aims to evaluate the corrosion performance of Al-Si as automotive alloys with varying concentrations of Si in deep seawater using electrochemical impedance spectroscopy and potentiodynamic polarization techniques. The surface condition prior to corrosion, as well as after corrosion, is analyzed using optical and scanning electron microscopy. The entire test is performed at an ambient condition. The results demonstrate that the corrosion resistance improves in alloys with increasing amounts of Si near the eutectic level, after which the corrosion protection deteriorates. Higher Si concentrations show higher values for polarization resistance and open circuit potential. In contrast, corrosion current and corrosion rate values decrease with increasing Si concentration up to eutectic composition. Si assists the formation of SiO_2 and MgO films through Mg_2Si intermetallics along with the Al_2O_3 on the surfaces, which aids in corrosion resistance. Optical and scanning electron micrographs reveal the presence of films on the surfaces after corrosion, which exhibit pits and pinholes on the surfaces of the alloys with lower Si concentrations. Hypereutectic alloy is affected by corrosion of its pinhole-like defects. The corresponding EDS analysis also confirms the protective layer of different oxides on the surfaces.

ARTICLE HISTORY
Received : 03rd Apr 2023
Revised : 05th Sept 2023
Accepted : 06th Oct 2023
Published : 31st Oct 2023

KEYWORDS
Al-Si automotive alloy;
Protective oxide layer;
Corrosion potential;
Polarization resistance;
Microstructure

1.0 INTRODUCTION

In the case of Al-Si alloys, the eutectic term is associated with a level close to 12.6 wt.%Si of the prime alloying element. Alloys with this level of low or high Si are called hypo-eutectic or hyper-eutectic, respectively [1]. In this alloy system, 5 to 23 wt.% Si is utilized; however, in the majority of situations, 6-7 wt.% is used as hypo-eutectic, 12-13 wt.% as eutectic, and 18-19 wt.% for hyper-eutectic are regarded. Binary Al-Si alloy does not offer good mechanical properties except excellent cast ability. To enhance the mechanical properties, minor alloying elements like Cu, Mg, Ni, Zn, and Mn are added to these alloys [2-4]. Also, the trace addition of Zr, Ti, Sc, and Ce in the alloy is considered a grain refiner [5, 6]. In addition, impurities such as Fe, Pb, and Sn are automatically added to the alloy by casting [7]. Among the various alloying elements, Cu and Mg are mostly considered due to their heat treatment properties. In a general sense, the best combination for automotive alloys is Al-Si-Cu-Mg alloy [8, 9]. The automotive industry focuses on lightweight materials like Al-Si alloys to make or manufacture automobile parts such as engine blocks, pistons, cylinder heads, intake manifolds, and others to replace cast iron [10-12]. They consider these alloys in this sector for good wear and corrosion performance. Automotive alloys have to work in different environments. More specifically, engine pistons and cylinders are constantly exposed to engine fuel. Often, several unanticipated chemical components may be mixed up with fuel as well as motor oil. When the alloys operate in a marine environment, particularly in ship engines, they can obviously be exposed to seawater. Hence, there is a possibility of corrosion of materials.

Corrosion can be defined as the gradual degradation of a material under chemical or electrochemical reactions in an exposed environment. Corrosion of engine parts results in deterioration of physical and mechanical properties, which impairs engine performance [11, 13, 14]. Many investigations are done with Al-Si automotive alloys where either natural corrosion or electrochemical corrosion processes are applied. At the same time, different alloying elements are added, and the different corrosive environment is considered for these investigations. It confirms that different environments, along with the alloying elements, greatly influence corrosion behavior. For most cases in saline environments, artificial seawater like 3.5wt% NaCl solution is used [15-17]. But for deep seawater, a complex mixture contains different types of salts along with NaCl, dissolved inorganic and organic matter, and minor atmospheric gases. So, the corrosion behaviour must be different in the seawater environment for different types of automotive alloys [18, 19].

Electrochemical corrosion properties under deep seawater on Al-Si automotive alloys have not been adequately studied considering the role of different Si. The present study covers the corrosion behavior of hypo-eutectic, eutectic and hyper-eutectic Al-based automotive alloys with impurities and minor additions of Si in two other alloys. To isolate the Si effect on this corrosion properties, the other alloying elements, like Cu, Mg, Fe, and Ni, are maintained constant. Investigations have been conducted by electrochemical impedance spectroscopy methods that are complementary to microscopy analysis.

***CORRESPONDING AUTHOR | M. S. Kaiser** | ✉ dkaiser.res@iubat.edu

2.0 EXPERIMENTAL METHOD

Al-Si-based hypoeutectic, eutectic and hypereutectic automotive alloys were considered for the electrochemical corrosion studies. Apart from Si and it at lower levels, two more alloys were taken into the study to get a clear idea. Minor alloying elements Cu and Mg were regularly alloyed to isolate the effect of Si on the corrosion behavior. For this purpose, Al-50 wt.% Si master alloy ingots along with commercially available pure aluminium, copper and magnesium, were used. The composition of the five test alloys was determined by Shimadzu PDA 7000 optical emission spectrometer, and the key elements are tabulated in Table 1.

Table 1. Elements by weight percent of the experimental five alloys

Alloy	Element (wt.%)						
	Al	Si	Cu	Mg	Fe	Ni	Others
Alloy 1	96.112	0.244	2.158	0.767	0.211	0.199	0.309
Alloy 2	92.552	3.539	2.309	0.784	0.273	0.217	0.326
Alloy 3	90.060	6.149	2.113	0.754	0.301	0.264	0.359
Alloy 4	83.424	12.656	2.130	0.770	0.311	0.277	0.432
Alloy 5	78.119	17.851	2.190	0.755	0.321	0.281	0.483

Graphite crucibles were used in a natural gas-fired pit furnace to cast the alloys. A conventional casting method was applied, and a suitable flux cover was used to avoid oxidation. In coarse casting, a mild steel metal mould of 20×200×300 mm preheated at 250 °C was used. Then, the five cast alloys were put into heat treatment by sequence 450 °C for 12 hours for homogenization, 535 °C for 2 hours for solutionizing and rapid cooling into salt water for quenching. Later, the alloys were machined to remove the surface oxide layer and 5×5×12 mm in size for corrosion study. Different grits of 320 to 2000 emery sheets were applied to the samples to get a smooth and finished surface. They were subjected to age hardening at 200 °C for 4 hours to obtain peak strength [5, 9]. A muffle furnace was used for all kinds of heat treatment processes of the alloys. The entire experiment was performed at an ambient condition of 70% humidity and 22°C temperature. Densities were considered from the chemical composition of the alloys.

Seawater was collected from the Bay of Bengal, specifically from a point in Saint Martin Island with coordinates of 20°37′30″N and 92°20′53″E. The seawater had a density of 1.024 g/cm^3 and a pH of 7.14 [19]. Electrochemical glass cells were used for corrosion analysis, with three electrodes: a working electrode, a reference electrode, and a counter electrode. The samples served as the working electrodes, the reference electrode was Ag|AgCl-KCl, and a platinum rod served as the counter electrode. The CH Instrument–Electrochemical Workstation was used for the overall electrochemical corrosion analysis. The glass cell was filled with 100 mL of seawater, and each sample was immersed in the cell before measuring the open circuit potential (OCP). The OCPs were determined by measuring the voltage between the working and reference electrodes. To perform the EIS analysis, a sinusoidal voltage with an amplitude of 5 mV was applied, and the frequency was swept from 100 kHz to 0.2 Hz. The electrolyte was replaced for each analysis. EIS was conducted at the OCP values previously measured, and impedance data were collected over the frequency range mentioned. The obtained data were used to design analogous electrical circuits with the data analysis program EC-Lab Analyst. The circuit with maximum accuracy was selected, and the values of the respective circuit components, such as solution resistance (RS), corrosion resistance (RP), and effective double-layer capacitance (CP(eff)), were calculated. For potentiodynamic polarization experiments, a similar setup as for the EIS was used. The potential range against the reference electrode was adjusted from -1.3 V to +0.6 V, and the scan rate was set at 0.50 mV s^{-1}. Following the experiment, Tafel polarization plots were generated, and the corrosion potential (E_{corr}) in mV, the corrosion current (I_{corr}) in μA, and the corrosion rate in millimeters per year were determined for each experimental alloy. Before and after the experiment, the surfaces were examined using both optical and scanning electron microscopes. The corrosion rate in mm year^{-1} is determined in accordance with ASTM Standard G 102 as:

$$\text{Corrosion rate} = \frac{I_{corr}\, K\, EW}{\rho\, A} \quad (1)$$

where I_{corr} = corrosion current (A), K = constant defining the units of corrosion rate in mm/year^{-1} (here, K = 3272 mm/A cm year), EW = equivalent weight (gm/equivalent), ρ = density of alloy (gm cm^{-3}) and A = surface area (cm^2). A USB digital microscope was selected for optical microscopy. Similarly, a JEOL scanning electron microscope attached to an x-ray analyzer was used for the SEM and EDX analysis.

3.0 RESULTS AND DISCUSSION

3.1 Impedance measurement

Table 2 displays the OCP values measured in the study, which demonstrate that increasing Si wt.% up to the eutectic composition around 12.7 Si wt.% leads to a more positive OCP, indicating improved corrosion resistance. This finding is consistent with previous studies linking a more positive OCP with better corrosion resistance [20]. Thus, the study suggests that increasing Si content enhances corrosion resistance in deep seawater as long as Si wt% does not exceed the eutectic level.

The EIS analysis measured impedance values that were compared with relevant electrical circuits, and the most excellent fitted circuit is shown in Figure 1. The polarization resistance (R_p), which is equivalent to charge transfer resistance, was found to be higher than the ohmic solution resistance (R_s) of the electrolyte. The polarization resistance of any material is inversely related to the corrosion rate and provides information about the rate of reactivity of the surface to the environment, as demonstrated in preliminary investigations [20, 21]. The study found that Rp increased from base Alloy 1 (0.2Si) to eutectic level Alloy 4 (12.7Si), indicating higher corrosion resistance in alloys with higher Si content. However, this trend was not followed in the case of hypereutectic Alloy 5 (17.9Si). The study suggests that the increased presence of Si in the alloys contributes to their improved corrosion resistance. During seawater corrosion, different oxides form protective layers that strongly bond to the surface, preventing further corrosion [22]. However, the primary silicon phase is formed ahead of the eutectic composition, which makes the alloy flaws, such as grooves and pinholes induce more corrosion in Alloy 5 [23].

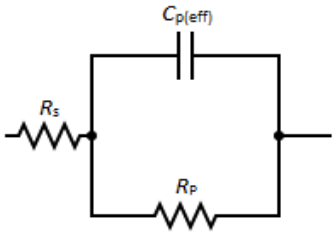

Figure 1. Used equivalent electrical circuit for fitting EIS data

Table 2. Results obtained from EIS and OCP values

Alloy	OCP, V vs. SCE	Rs / Ω	Rp / Ω	Cp(eff) / µF	Goodness of fit
Alloy 1 (0.2Si)	-0.84136	30.26	13771	13.53	0.0060870
Alloy 2 (3.5Si)	-0.84038	27.94	19769	8.018	0.0008761
Alloy 3 (6.1Si)	-0.83968	24.28	27776	5.677	0.0031180
Alloy 4 (12.7Si)	-0.83028	23.56	37842	2.189	0.0058510
Alloy 5 (17.9Si)	-0.85241	41.9	33925	2.047	0.0003099

Figure 2 gives an idea about the Nyquist diagram through the impedance values of different Si-doped automotive alloys immersed in seawater. The x and y axes stand for the real (Z_{real}) and imaginary ($Z_{imaginary}$) parts, respectively, of the impedance behaviour. The imaginary component of the impedance alongside the real part is derived by applying the capacitive-resistive model. The semicircular shape of each alloy in the Nyquist diagram indicates that Al-Si automotive alloy corrosion is controlled by charge transfer mechanisms. Frequency dispersion causes small distortions in the image, as observed [21, 24]. They also indicate not perfect semicircles, as expected by EIS theory, since the non-ideal behavior of the double-layer capacitor [25]. Both the real and imaginary parts of the impedance increase for the alloys with higher Si concentration up to the eutectic level. It may be clarified that the formation of an oxide layer on the surfaces increases the impedance for both. Higher Si means higher oxide formation, which normally forms the oxide layer of Al.

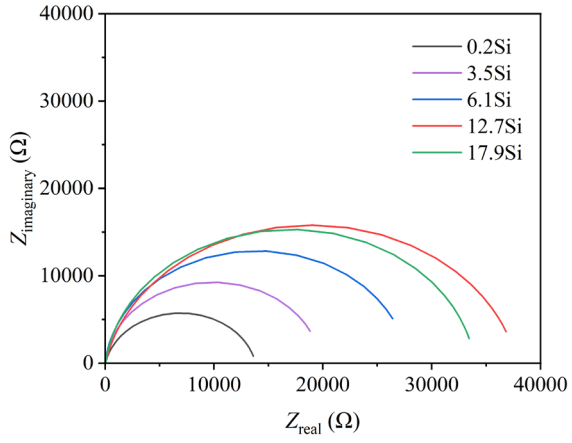

Figure 2. Nyquist plots for the five alloys alloys tested in deep sea water at room temperature

Nyquist plot has the limitation that it does not display the precise frequencies on which the impedance value is considered. This limitation can be overcome by showing the frequency specific impedance behavior of the system by plotting the Bode plot [26]. The impedance data obtained from the electrochemical corrosion of different Si-added automotive alloys in deep sea water are displayed as Bode plots in Figure 3. The Bode magnitude plot demonstrates the impedance modulus versus frequency in Figure 3(a), and the Bode phase plot displays the phase angle versus frequency as in Figure 3(b). It is seen from the magnitude plots that at the low frequency, the impedance modulus (/Z/) is lower for the lower Si added alloys and increases with the Si contents, which means higher protection against corrosion through the

formation of the oxide layer. It can be seen from the phase angle plots the impedance spectra represent two-time constants. The two-time constants can be assigned to the electron charge transfer process across the double layer at the interface and to the native oxide layer. In the case of Si addition, the second time constant associated with the Bode phase angle plot is extended over a wide range of frequencies, revealing that it is composed of aluminum oxide layer resistance. The frequency spread of the phase angle is maximum in the presence of higher Si in the alloy. Hypereutectic alloy is restricted to graphs showing inferior frequencies.

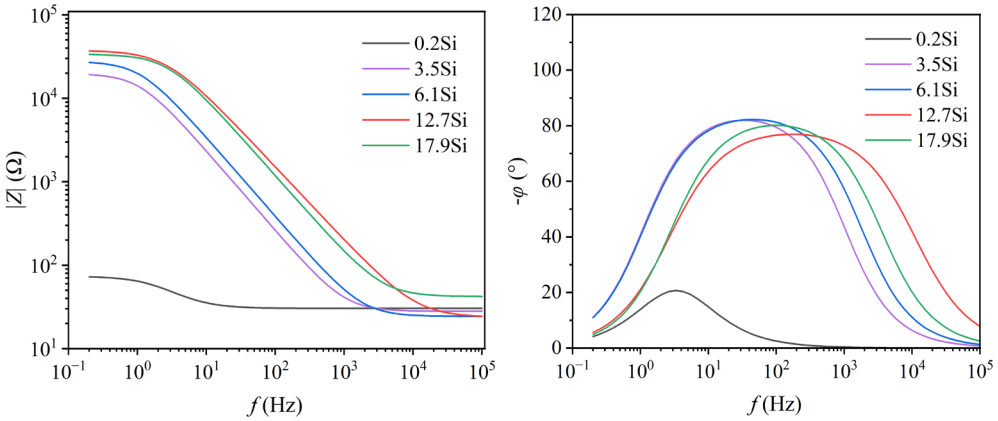

(a) impedance modulus |*Z*| vs. frequency (b) phase angle vs. frequency

Figure 3. Bode plots for different Si-added automotive alloys

3.2 Potentiodynamic Polarization Analysis

Figure 4 shows the polarization curves of the Tafel plots of the tested five Al-Si automotive alloys with various levels of Si concentration in deep seawater. These curves each demonstrate similar shapes consisting of cathodic and anodic branches. The little scatter in the potentiodynamic curves may be due to the nature of the surfaces of alloys, such as porosity, internal cracks, un-melted powder, and the absorption of melt pool borders [27]. The curves associated with higher Si up to eutectic level move towards a positive direction in terms of corrosion potential. The parameters of corrosion current densities (I_{corr}), corrosion potentials (E_{corr}), and corrosion rate are obtained by Tafel plots using both cathodic and anodic branches of the polarization curves. These values are plotted against the Si content in the alloys for better clarification of the typical electrochemical corrosion characteristics.

Figure 5 displays the behavior of both I_{corr} and E_{corr} with changes in the Si content of the alloys. This figure clearly displays that values of I_{corr} decrease with Si content up to the eutectic level and then increase drastically with Si content. The E_{corr} value shows the opposite phenomenon of it. The corrosion current is represented as I_{corr}, which is directly involved with the dissolution of corroded product. Si addition protects the dissolution of the surface material by providing the oxide layer so the decrees in this I_{corr} values. On the other hand, E_{corr}, the corrosion potential, also known as the open circuit potential, is the mixed potential where the rate of anodic dissolution equals the rate of cathodic reaction, with no net current flowing into or out of the electrodes. E_{corr} represents the ability of metal and nonmetal surfaces to lose electrons in the presence of electrolyte corrosion.

The corrosion rate of a material is the key parameter normally denoted as mm/year to express the result of this process. The corrosion rate changed with the Si contents of the alloys in Figure 6, which follows the same trend of corrosion current densities as directly related. The overall aspects of the process can be explained more specifically and in detail in the following manner. As the alloys are used at their peak aged condition, these types of alloys consist of various intermetallics like Al_2Cu, Mg_2Si along with $Al_5Cu_2Mg_8Si_6$, $Al_9FeMg_3Si_5$, β-Al_5FeSi phases and so on. However, the first two intermetallics phases are mainly responsible for strengthening the alloys [28]. Whereas the base alloy contains a negligible amount of Si the intermetallic rich in element Mg, that is Al_2CuMg and Al_3Mg_2 are anodic relative to the matrix Al, as high potential anodic dissolvers. The intermetallic containing Cu and Fe, like Al_2Cu, Al_5Fe_2 promote dissolution of the matrix because intermetallic potential is lower than that of Al element, mainly because Al dissolves preferentially. When the Al matrix surrounding the intermetallic is completely dissolved, the intermetallic was exfoliated from the surface of the sample. Generally, Al alloy under electrochemical corrosion in corrosive media forms Al_2O_3 on the surface, which normally protects the alloy from corrosion [29]. Silicon provides better resistance to the passive film, resulting in less pitting corrosion, as previously reported. With increasing the Si level in the alloys, these additional phases can reasonably affect the corrosion performance. The intermetallics Mg_2Si acts as an anode and is dissolved preferentially. Conversely, Mg_2Si with water forms oxides like SiO_2 and MgO, which is widespread. As a result, it protects the Mg_2Si particles and reduces the galvanic coupling with the aluminium matrix. Additionally, Si may allow the forming of the interdiffusion layer Al_5FeSi phase, which limits the growth of iron-rich intermetallics Al_5Fe_2. Such intermetallic layers only provide the barrier but do not give the cathodic protection [30]. The exception is observed in hypereutectic alloy as beyond the eutectic composition, more star-shaped blocky primary Si along with needles or plate-like eutectic Si are created in the matrix. During solidification, these Si particles distribute randomly, and the interface creates different sizes

of pits, pinholes, surface step- or groove-like interfaces, burrs and necks along the particle surface of the alloys [23]. As a result, excess corrosion easily occurs in areas where there are holes or cracks.

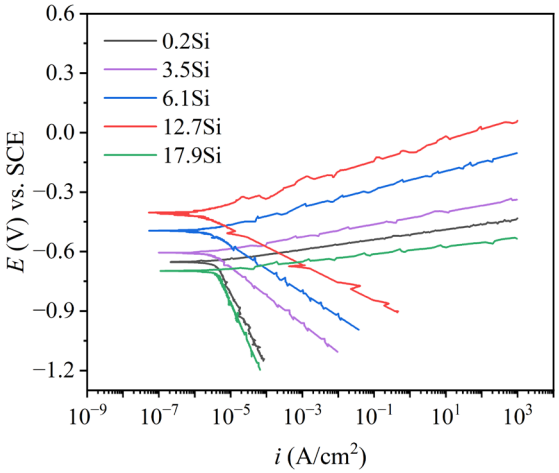

Figure 4. Potentiodynamic polarization curves of five alloys tested in deep seawater

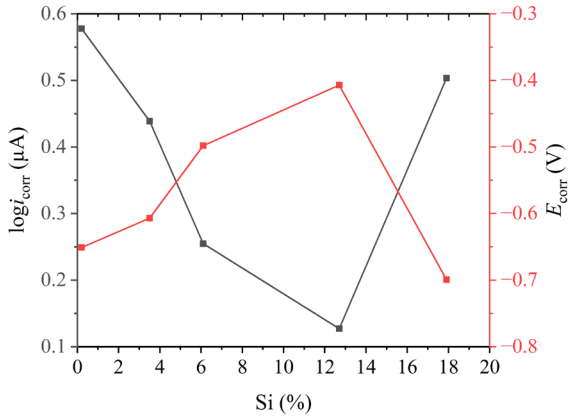

Figure 5. Corrosion current density and potential deviation of the automotive alloys with varying levels of Si in deep seawater

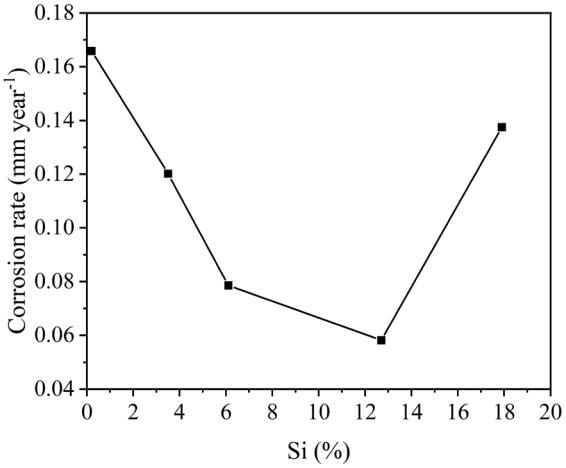

Figure 6. Changes in corrosion rate of the automotive alloys with varying levels of Si in deep seawater

3.3 Optical Micrographic Investigation

The worn surfaces of the alloys before corrosion as well as after corrosion in seawater are displayed in Figure 7. Before corrosion of the alloys without etchant, the polished surfaces do not offer enough information regarding the microstructures but show the appearance of some variation with only lighter tones and darker tones. There are also slight scratches on the surface due to polishing. Generally, these types of alloys consist of Al-rich dendrites matrix distributed with different intermetallic phases formed by the elements. When Si is added, the eutectic Si phase starts to come into the microstructures. At the eutectic composition, elongated needle-like and platelet eutectic silicon phases are formed, and in

the case of hypereutectic composition, additional star-shaped blocky primary Si is formed [2, 31, 32]. Precipitates with different intermetallics appear in a darker tone, whereas Si-rich intermetallics appear in a lighter tone. Thus, with different amounts of Si, the alloy's microstructure exhibits various levels of tone.

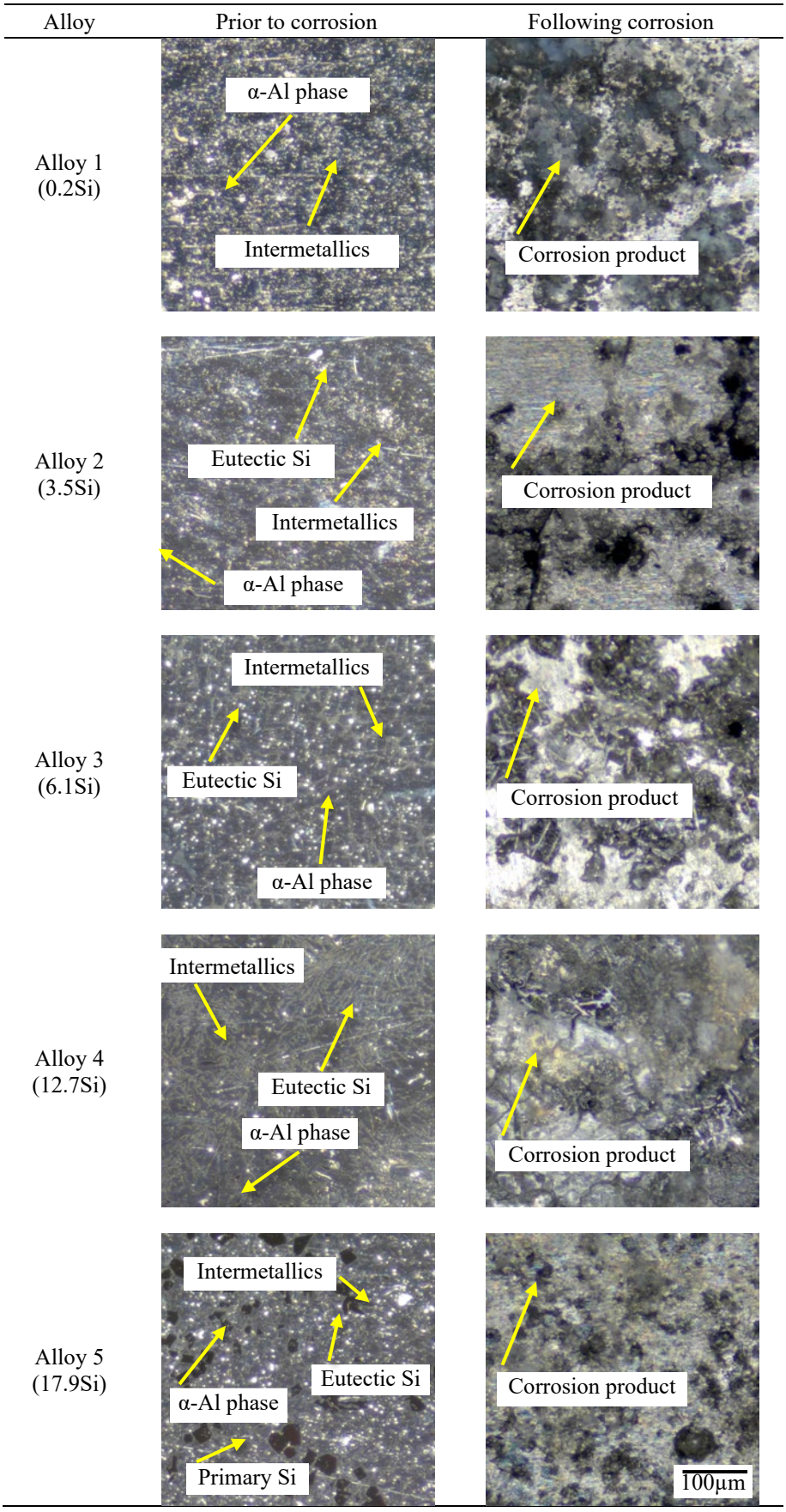

Figure 7. Microstructure of five alloys prior to corrosion and after corrosion in deep seawater

Subsequent to the electrochemical corrosion process, the test alloys are corroded on the surface at different intensities depending on the Si concentration level in the alloys. It may be attributed to the fact that higher levels of Si form a higher protective oxide layer, which controls the degradation of the surfaces. There are no signs of polishing scratches and different tones due to the formation of corrosion oxide layers on the surfaces [33]. The surface's appearance is somewhat different due to the composition of seawater being composed of different elements and different levels of intermetallic created by varied Si. Hypereutectic alloy consists of some spots uniformly distributed on the surface since the additional pit formation in the region of the primary Si on the surfaces.

3.4 SEM and EDX Observations

Figure 8 shows the SEM images with EDX spectra of the investigated surface morphologies after the test of electrochemical corrosion in deep seawater. The five alloy images confirm the corrosion products associated with various intermetallic compounds on the alloy surfaces. Isolated pits with localized corrosion are visible on the surfaces also. The intensity of these pits and attacks are higher for lower Si added alloy, and it reduces with the Si concentration in the alloys. Up to eutectic composition, the alloys show excellent performance, but beyond this composition the hypereutectic level drastically falls the property. The whole thing can be certified to the formation of Al oxide along with other oxide layers on the surface during the electrochemical corrosion process, which protects the dissolution of the surface material. The addition of Si helps to form other oxide layers of Mg and Si on the surface. This layer is relatively stable and provides good protection, hence less dissolution as well as lower pit formation. It has already been stated that conventional cast hypereutectic alloys are always prone to defects such as pin holes, micro cracks due to the presence of unmodified primary Si in Al-matrix. These voids facilitate corrosion by internal damage, as clearly seen by the surface of hypereutectic alloy [15].

The EDX data of corroded surfaces also be conventional to the corrosion behavior of alloys. It can be seen from Table 3 that the percentage of oxygen decreases with the addition of Si in the alloys. This means the continuous attack is higher for lower Si-doped alloys, as well as continuous dissolution corrosion rate increases. Hypereutectic alloy too follows this trend of oxidation but is damaged by defects such as porosity, which are clearly visible through the microstructure of Alloy 5. Another observation is that by subtracting the oxide levels from the wt.% obtained chemical composition by optical emission spectrometer, the corroded surface contains more wt.% Si. Although supplementary materials are dissolved in solution, the increased Si does not dissolve and forms Mg_2Si, which is concerned with protecting the material surfaces from corrosion, as stated earlier. It is clear to all that seawater is a heterogeneous mixture of about 96.5% water, 2.5% various salts and other substances, including small amounts of dissolved inorganic and organic matter and small atmospheric gases. Additionally, the most abundant ions are Cl^-, Na^+, SO_4^{2-}, Mg^{2+}, B^{3+} Ca^{2+} and K^+ [34]. Table 3 as well corroborates by displaying the elements like Br, Na, S, Cl, K, and Ca. These elements display more or less high for the higher Si-added alloys for better corrosion protection. Possible grounds are that Si helped to form different oxides, but corrosion is not similarly protected to form surface defects in hypereutectic alloys.

Table 3. EDX analysis of the alloy surfaces by wt.% after electrochemical test

Alloy	O	Al	Si	Cu	Mg	Fe	Br	Na	S	Cl	K	Ca
Alloy 1 (0.2Si)	60.71	19.03	0.02	0.57	0.66	0.01	11.67	5.84	0.40	0.26	0.56	0.27
Alloy 2 (3.5Si)	60.59	24.38	0.40	0.20	0.12	0.29	11.00	2.39	0.17	0.27	0.04	0.15
Alloy 3 (6.1Si)	59.75	25.92	1.01	0.30	0.25	0.44	9.27	2.37	0.14	0.31	0.20	0.04
Alloy 4 (12.7Si)	55.73	21.72	5.74	0.98	0.63	1.24	5.14	5.94	0.64	0.75	0.73	0.76
Alloy 5 (17.9Si)	54.58	17.60	7.29	1.22	0.88	0.04	10.31	5.48	0.57	0.65	0.48	0.90

(a)

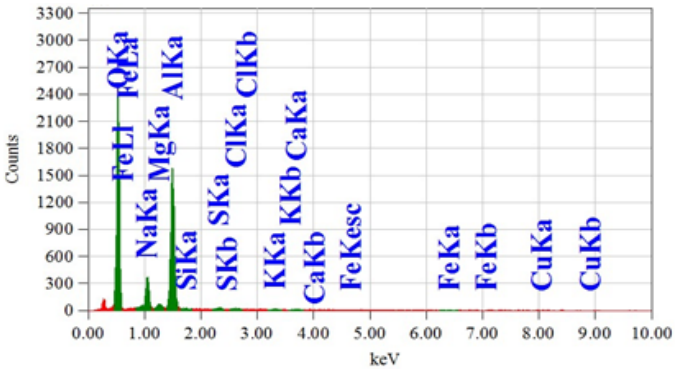

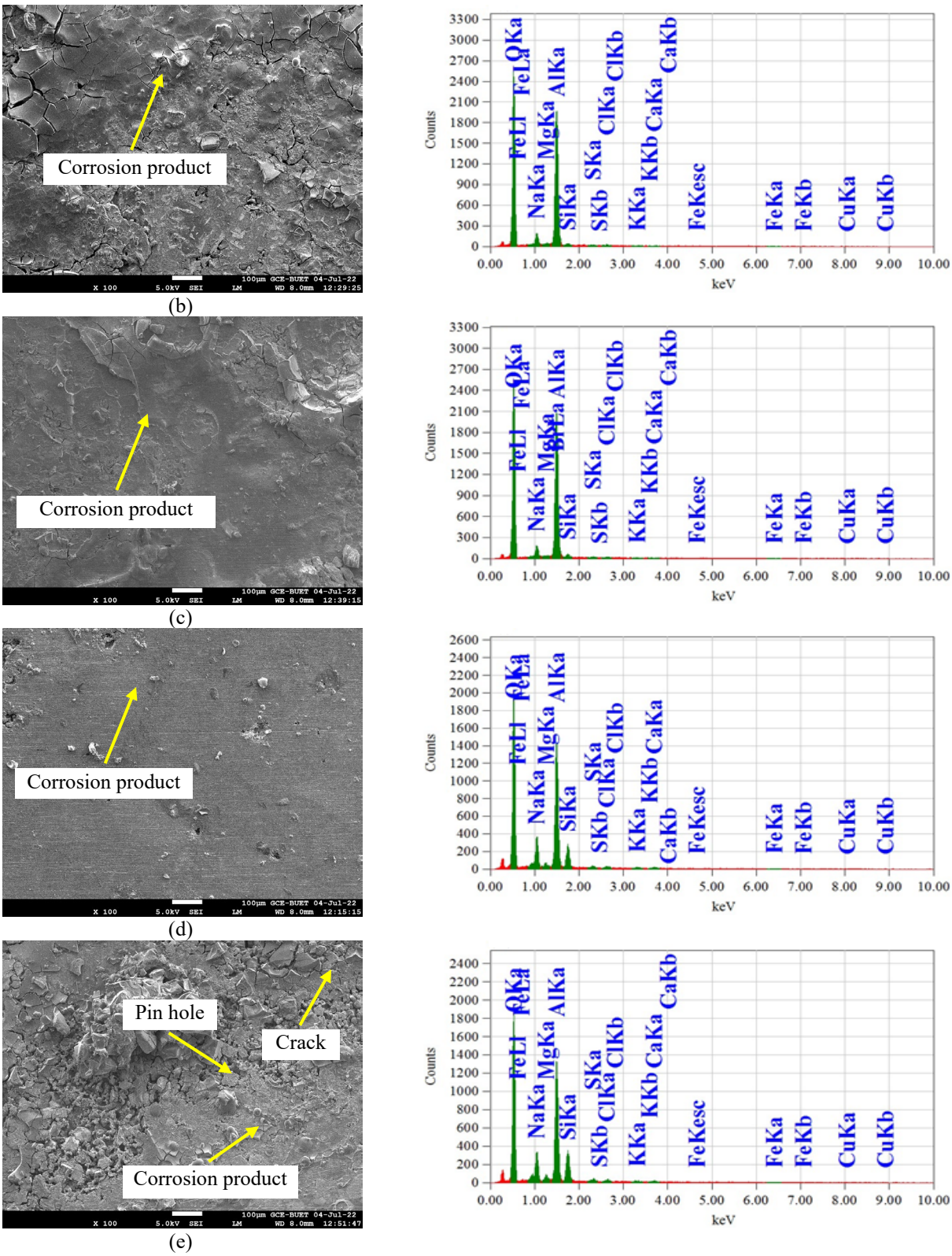

Figure 8. SEM images and EDX spectra of five different Si-doped automotive alloys after exposure to deep seawater: (a) 0.2Si, (b) 3.5Si, (c) 6.1Si, (d) 12.7Si, and (e) 17.9Si

4.0 CONCLUSIONS

Based on the above results of hypoeutectic, eutectic and hypereutectic Al-Si automotive alloys regarding the electrochemical corrosion performance in deep seawater, it is likely to draw the following conclusions:

The corrosion resistance of Al-Si automotive alloys improves with Si content at eutectic composition levels while the various alloying elements remain more or less the same. The formation of Al_2O_3 with other oxide layers protects the surface from corrosion. Alloys with higher Si provide higher protection through additional SiO_2 and MgO films across the intermetallic Mg_2Si. With higher Si beyond eutectic composition, elongated platelets primary Si along with Fe-

intermetallic typically form that produce surface macro-cracks and pinhole-like digression resulting in lower corrosion efficiency. The worn surfaces of alloys before corrosion show different tones due to the presence of various elements, but after corrosion, these are absent through the formation of corrosion layers. The surface of the hypereutectic Al-Si automotive alloys exhibits higher surface damage for its pinhole-like defects. The SEM images along with EDX spectra, confirm the higher percentage of oxygen on the surface of lower Si-doped alloys, which desolated continuously. It also verifies the elements as seawater contains different types of salts, inorganic and organic substances, and atmospheric gases. The combined alloying elements are higher for higher Si-added alloys because of their protective nature and smooth surface also visible.

5.0 ACKNOWLEDGEMENT

Thank you to both Department of Chemistry and Mechanical Engineering, Bangladesh University of Engineering and Technology, Dhaka, for necessary support. The corresponding author would like to express his gratitude towards the Director of Administration of IUBAT, for her efforts in fostering collaborations with other institutions have also been commendable.

6.0 REFERENCES

[1] Y. D. Jia, L. B. Zhang, P. Ma, S. Scudino, G. Wang, *et al.*, "Thermal expansion behavior of Al–xSi alloys fabricated using selective laser melting," *Progress in Additive Manufacturing,* vol. 5, no. 3, pp. 247–257, 2020.

[2] I. J. Polmear, *Light alloys-metallurgy of the light metals*, 3rd Edition*,* London, UK: Arnold, 1995.

[3] M. S. Kaiser, S. H. Sabbirb, M. S. Kabir, M. Rahman, and M. A. Nur, "Study of mechanical and wear behaviour of hyper-eutectic Al-Si automotive alloy through Fe, Ni and Cr addition," *Materials Research,* vol. 21, no. 4, pp. 1-9, 2018.

[4] M. G. C. Xavier, B. J. M. Freitas, G. Y. Koga, and J. E. Spinelli, "Effects of Ni and Co on the corrosion resistance of Al-Si-Cu-Zn-Fe alloys in NaCl solution," *Metals,* vol. 12, no. 645, 1-18, 2022.

[5] Y. Li, X. Du, J. Fu, Y. Zhang, Z. Zhang, *et al.*, "Microstructure and mechanical properties of Al–Si–Mg–Cu–Ti alloy with trace amounts of scandium," *Materials Science and Technology,* vol. 34, no. 10, pp. 1265-1274, 2018.

[6] S. K. Shaha, F. Czerwinski, W. Kasprzak, J. Friedman, and D. L. Chen, "Effect of Cr, Ti, V, and Zr micro-additions on microstructure and mechanical properties of the Al-Si-Cu-Mg Cast Alloy," *Metallurgical and Materials Transactions A*, vol. 47, pp. 2396-2409, 2016.

[7] M. S. Kaiser, "Effect of trace impurities on the thermoelectric properties of commercially pure aluminium," *Materials Physics and Mechanics,* vol. 47, no. 4, pp. 582-591, 2021.

[8] P. Zhou, D. Wang, H. Nagaumi, R. Wang, X. Zhang, *et al.*, "Microstructural evolution and mechanical properties of Al-Si-Mg-Cu cast alloys with different Cu contents," *Metals,* vol. 13, no. 98, pp. 1-13, 2023.

[9] S. Toschi, "Optimization of A354 Al-Si-Cu-Mg alloy heat treatment: effect on microstructure, hardness, and tensile properties of peak aged and overaged alloy," *Metals*, vol. 8, no. 11, 1-16, 2018.

[10] ASM Handbook, "Properties and selection of aluminum alloys," in *Volume 2B, ASM Handbook,* K. Anderson, J. Weritz, and J. G. Kaufman, Eds. Materials Park, Ohio, USA, 2019, pp. 46-51.

[11] ASM Handbook, "Friction, lubrication and wear technology," in *ASM Handbook,* G. E. Totten, Ed. Materials Park, Ohio, USA, 1992, pp. 57-69.

[12] H. Ye, "An overview of the development of Al-Si-Alloy based material for engine applications," *Journal of Materials Engineering and Performance,* vol. 12, pp. 288-297, 2003.

[13] A. A. Khan, and M. S. Kaiser, "Wear studies on Al-Si automotive alloy under dry, fresh and used engine oil sliding environment," *Research on Engineering Structures and Materials,* vol. 9, no. 1, pp. 1-18. 2023.

[14] E. Canepa, R. Stifanese, L. Merotto, and P. Traverso, "Corrosion behaviour of aluminium alloys in deep-sea environment: A review and the KM3NeT test results," *Marine Structures,* vol. 59, pp. 271-284, 2018.

[15] M. A. Nur, A. A. Khan, S. D. Sharma, and M. S. Kaiser, "Electrochemical corrosion performance of Si-doped Al-based automotive alloy in 0.1 M NaCl solution," *Journal of Electrochemical Science and Engineering*, vol. 12, no. 3, pp. 565-576, 2022.

[16] ASM Technical Books, "Corrosion of aluminum and aluminum alloys," in *ASM International,* J.R. Davis, Ed. Materials Park, Ohio, USA, 1999, pp. 25-40.

[17] A. S. Fouda, F. S. Mohamed, and M. W. E. Sherbeni, "Corrosion inhibition of aluminum–silicon alloy in hydrochloric acid solutions using carbamidic thioanhydride derivatives," *Journal of Bio- and Tribo-Corrosion,* vol. 2, no. 11, pp. 1-16, 2016.

[18] H. U. Sverdrup, M. W. Johnson, and R. H. Fleming, *The oceans: Their physics, chemistry, and general biology*, *15th Edition.,* New Jersey, USA: Prentice-Hall, Inc., 1942.

[19 M. M. Rahman, S. R. Ahmed, and M. S. Kaiser, "Corrosion behavior of work hardened SnPb-Solder affected copper in the Bay of Bengal water environment," *Advances in Materials Science and Engineering*, vol. 2022, pp. 1-14, 2022.

[20] S. Choudhary, A. Garg, K. Mondal, "Relation between open circuit potential and polarization resistance with rust and corrosion monitoring of mild steel," *Journal of Materials Engineering and Performance*, vol. 25, no.7, pp. 2969-2976, 2016.

[21] J. Bessone, C. Mayer, K. Jüttner, W. J. Lorenz, "*AC*-impedance measurements on aluminium barrier type oxide films," *Electrochimica Acta*, vol. 28, no. 2, pp. 171-175, 1983.

[22] D. Stathokostopoulos, D. Chaliampalias, E. Pavlidou, K. M. Paraskevopoulos, K. Chrissafis, and G. Vourlias, "Oxidation resistance of magnesium silicide under high-temperature air exposure," *Journal of Thermal Analysis and Calorimetry,* vol. 121, pp. 169-175, 2015.

[23] K. Chandra, and V. Kain, "Brittle failure of hypereutectic Al–Si alloy component," *Journal of Failure Analysis and Prevention*, vol. 15, pp. 679-85, 2015.

[24] W. Li, X. Chen, and B. Chen, "Effect of aging on the corrosion behavior of 6005 Al alloys in 3.5 wt% NaCl aqueous solution," *Journal of Materials Research*, vol. 33, pp. 1830-1838, 2018.

[25] J. Shi, Q. Hu, X. Zhao, J. Liu, J. Zhou, *et al.*, "Densification, microstructure and anisotropic corrosion behavior of Al-Mg-Mn-Sc-Er-Zr alloy processed by selective laser melting, *Coatings,* vol. 13, no. 337, pp. 1-15, 2023.

[26] V. Vivier and M. E. Orazem, "Impedance analysis of electrochemical systems," *Chemical Reviews,* vol. 122, no. 12, pp. 11131-11168, 2022.

[27] R. I. Revilla, D. Verkens, T. Rubben and I. D. Graeve, "Corrosion and corrosion protection of additively manufactured aluminium alloys—A critical review, *Materials,* vol. 13, no. 4804; pp. 1-25, 2020.

[28] A. M. A. Mohamed, E. Samuel, Y. Zedan, A. M. Samuel, H. W. Doty and F. H. Samuel, "Intermetallics formation during solidification of Al-Si-Cu-Mg cast alloys," *Materials,* vol. 15, no. 1335, pp. 1-24, 2022.

[29] M. Cao, L. Liu, L. Fan, Z. Yu, Y. Li, *et al.*, "Influence of temperature on corrosion behavior of 2A02 Al alloy in marine atmospheric environments," *Materials,* vol. 11, no. 235, pp. 1-22, 2018.

[30] R. E. Lozan, M. I. P. Canul, M. A. P.Canul, M. M. Dávila, and A. U. Salas, "The role of Mg2Si in the corrosion behavior of Al-Si-Mg alloys for pressureless infiltration," *The Open Corrosion Journal*, vol. 3, pp. 73-79, 2010.

[31] B. Zhang, L. Zhang, Z. Wang, and A. Gao, "Achievement of high strength and ductility in Al–Si–Cu–Mg alloys by intermediate phase optimization in as-cast and heat treatment conditions," *Materials (Basel)*, vol. 13, no. 3, pp. 1-14, 2020.

[32] B. Jiang, S. Xu, H. Y. Xu, M. L. Hu, Y. J. He, and Z. S. Ji1, "Effect of Mg addition on microstructure and mechanical properties of Al-Si-Cu-Fe alloy with squeeze casting," *Materials Research Express,* vol. 7, no. 1, pp. 1-9, 2019.

[33] M. S. Kaiser, M. R. Qadir, and S. Dutta, "Electrochemical corrosion performance of commercially used aluminium engine block and piston in 0.1M NaCl," *Journal of Mechanical Engineering, The Institution of Engineers, Bangladesh,* vol. 45, no. 1, pp. 48-52, 2015.

[34] K. C. Kang, P. Linga, K. Park, S. J. Choi, and J. D. Lee, "Seawater desalination by gas hydrate process and removal characteristics of dissolved ions (Na+, K+, Mg2+, Ca2+, B3+, Cl-, SO42-)," *Desalination,* vol. 353, no. 13, pp. 84-90, 2014.